

Adaptive-Optic Correction of a Regularized Compressible Shear Layer

Alice Nightingale^{*}, Daniel A. Duffin[†], Michael Lemmon⁺, Bill Goodwine[‡], and Eric J. Jumper[§]
Center for Flow Physics and Control
University of Notre Dame, Notre Dame, IN 46556

Non-uniform, variable-density fields, resulting from compressibility effects in turbulent flows, are the source of aero-optical distortions which cause significant reductions in optical system performance. Adaptive-Optics (AO) is a technique used to correct for such spatially and temporally varying aberrations on an optical beam by applying a conjugate waveform correction to the beam. Traditional AO systems are bandwidth limited by real-time processing issues and wavefront sensor limitations. This paper presents an alternative AO approach using a phase-locked-loop control strategy. By using flow control to regularize the shear layer and its corresponding optical wavefront, the bandwidth necessary to make real-time corrections is effectively reduced by producing a more periodic and predictable optical signal. A feedback control approach has been simulated numerically performing real-time corrections to an aberrating wavefront due to propagation through a free shear layer. Several cases were studied for a variety of upper and lower Mach numbers. The numerical results show significant increases in the time-averaged Strehl ratio for the cases where the regularized wavefront contained a single dominant frequency. Further increases in the Strehl ratios were achieved after additionally removing tip/tilt. It was noted that tip/tilt error must be removed post AO corrections rather than prior in order to maintain a traveling wavefront necessary for this control strategy. In the highest Mach number case studied, regularization of the shear layer produced an optical wavefront containing both fundamental and subharmonic frequencies. Higher Mach number cases, such as this, may require the use of two frequency control which is currently being investigated further.

Nomenclature

OPL	=	Optical Path Length
OPD	=	Optical Path Difference
n	=	index-of-refraction
p	=	pressure
ρ	=	density
u	=	velocity in x direction, along the streamwise direction
v	=	velocity in y direction, perpendicular to the flow direction
T	=	temperature
T_{ad}	=	initial temperature calculated using the adiabatic relation
p_{∞}	=	free stream pressure
γ	=	specific heat ratio
θ	=	jitter angle
f_n	=	optical natural frequency
A_n	=	optical coherence length
U_c	=	convective velocity

^{*} Graduate Research Assistant, DEPS Fellow, Student Member AIAA

[†] Graduate Research Assistant, NDSEG Fellow, Student Member AIAA

⁺ Professor

[‡] Professor

[§] Professor, AIAA Fellow

I. Motivation

Optical systems, including free-space communication platforms and airborne laser weapon systems, transmit and receive optical signals that must propagate through variable density flow fields which adversely affect the system's performance. Figure 1 shows an example of a variable-density shear layer forming as the air separates across an airborne turret.¹

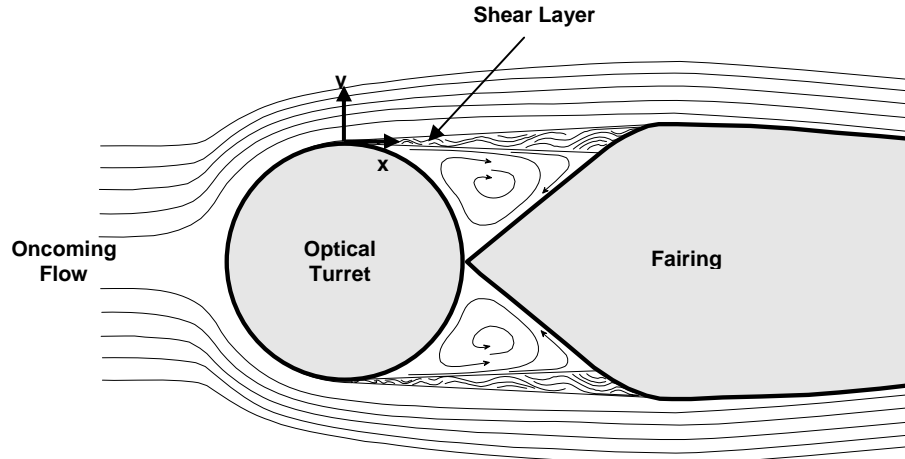


Figure 1. Shear layer formed over a turret/fairing combination.

Variations in the flow field density and its concomitant index-of-refraction are due to coherent turbulent structures, loosely referred to as compressibility effects.² When a collimated laser beam is propagated through such a variable index-of-refraction flow field, the beam's optical wavefront becomes aberrated. These aberrations are commonly quantified using optical path length (OPL) and optical path difference (OPD). $OPL(t,x)$ is defined as the integral through a variable index-of-refraction field, $n(t,x,y)$, along the path a ray travels. Due to small deviations in the ray's path from the initial direction of propagation, $OPL(t,x)$ can be approximated by integrating along this axis (y -axis shown in Figure 1);

$$OPL(t, x) = \int_{\text{ray}} n(t, x, y) ds \approx \int_{y_1}^{y_2} n(t, x, y) dy \quad (1)$$

$OPD(t,x)$ is calculated by removing the spatial mean ($\overline{OPL}(t_o)$) at each time step producing,

$$OPD(t_o, x) = OPL(t_o, x) - \overline{OPL}(t_o) \quad (2)$$

Adaptive Optics (AO) is the technique of applying the conjugate waveform to the optical wavefront prior to its transmission through an aberrating medium, effectively restoring a planar wavefront.³ Traditional AO systems are commonly comprised of a Wavefront Sensor (WFS), Conjugate Constructor (CC), and deformable mirror (DM). The WFS measures the aberration, the CC constructs the appropriate conjugate correction, and the DM applies the correction to the wavefront. Due to system stability and the bandwidth requirement set by the aberrating flow field itself, aberrations must be detected and measured at a rate one hundred times that of the disturbance bandwidth.^{3,4,5} In high-speed applications, such aberrations commonly occur at frequencies above 1 kHz, which exceeds current AO system capabilities.⁶ This paper examines the possibility of using flow control in conjunction with an alternative AO control approach to overcome these bandwidth limitations.

II. Numerical Model

The results presented in this paper were obtained using a numerical model that simulates two flows of different velocity, but identical total temperature, on either side of a stationary splitter plate; the flows merge to form a free shear layer. The model starts by calculating the unsteady velocity field using a

discrete vortex method. A thermodynamic overlay is then used to determine the thermodynamic properties from the computed velocity field. The following sections provide a more detailed description of each step.

A. Discrete Vortex Method (DVM)

Several inviscid and pseudo-inviscid methods have been successfully used to model rollups in a shear layer caused by the Kelvin-Helmholtz instability mechanism.^{7,8,9} The current study was performed using a pseudo-inviscid, two-dimensional discrete vortex method (DVM) developed at Notre Dame.^{2,10} The shear layer is modeled using two semi-infinite vortex sheets, solved analytically, on either side of a finite vortex sheet solved numerically (computational domain). The splitter plate is simulated using a string of positionally-fixed vortices while the remaining vortices within the computational domain are allowed to move and convect based on the induced velocity from all other vortices and the overall convective velocity. The rotational core associated with each discrete vortex is modeled using a temporal growth rate, simulating momentum diffusion. The model also uses vortex insertion when two adjacent vortices exceed a specified distance apart to ensure stability.¹¹

B. Weakly-Compressible Model (WCM)

Once the velocity field is available from the DVM, another numerical code, designated the *Weakly-Compressible Model* (WCM), is used to overlay the thermodynamic properties onto the velocity field. The unsteady Euler equations,

$$\begin{aligned}\frac{\partial p}{\partial x} &= -\rho \left[\frac{\partial u}{\partial t} + u \frac{\partial u}{\partial x} + v \frac{\partial u}{\partial y} \right] \\ \frac{\partial p}{\partial y} &= -\rho \left[\frac{\partial v}{\partial t} + u \frac{\partial v}{\partial x} + v \frac{\partial v}{\partial y} \right]\end{aligned}\quad (3)$$

are back solved using a four-point central difference scheme to calculate the pressure gradients from which the pressure field is computed. The adiabatic heating/cooling equation and the perfect gas law are used to find the initial temperature and density fields. These iterations are repeated until the density field converges. At this point another iteration loop is run using the Hilsch approximation,

$$\frac{T(t, x, y)}{T_{ad}(t, x, y)} = \left(\frac{p(t, x, y)}{p_{\infty}} \right)^{\frac{\gamma-1}{\gamma}}, \quad (4)$$

to solve for the temperature variations within the flow field. The density iteration cycle is then repeated followed by the temperature iteration cycle until pressure, density, and temperature converge at each time step.^{2,10} The index-of-refraction field, $n(t, x, y)$, is determined using the Gladstone-dale constant from which the OPL and OPD are computed using Eq. (1) and Eq. (2). According to Huygen's Principle, small aperture beams propagating through a variable flow field emerge normal to the optical wavefront. Therefore, since the wavefront aberrations are both spatially and temporally varying, the angle at which a small aperture laser beam emerges from the flow will similarly vary in time and with each spatial location. This angle, $\theta(t, x_o)$, referred to as jitter angle, is defined as,

$$\theta(t, x_o) \cong - \left. \frac{dOPD(t, x)}{dx} \right|_{x_o}. \quad (5)$$

Once the optical wavefronts are obtained, far field diffraction patterns are calculated using the Fraunhofer approximations. The Strehl ratio, St , defined as the ratio of actual on-target intensity to diffraction limited on-target intensity, is commonly used to quantify system performance. For a perfectly planar wavefront producing maximum on-target intensity, a Strehl ratio of 1.0 is achieved.

The results obtained using the DVM and WCM have been found to be in good agreement with experimental results. Good comparison between mean velocity profiles from the numerical model and an

incompressible and weakly-compressible experimental shear layer validate the DVM computations. The vorticity thickness growth rate also showed good comparison with the growth rate predicted in literature.² Flow visualization and pressure measurements presented by Fitzgerald and Jumper (2004) show validation of the WCM results.^{2,12} The following sections discuss results obtained from numerical simulations using the DVM and WCM.

III. Shear Layer Regularization

In a numerical study performed by Nightingale et al. (2005), it was shown that vortical structures in a shear layer may be regularized by applying a forcing mechanism to its origin within the range of its optical “natural” frequencies.⁴ This regularizing effect concurs with the results found by Oster and Wygnanski (1982) for a forced mixing layer.¹³ An unforced shear layer contains a range of inherent optical “natural” frequencies defined as

$$f_n(x) = \frac{\int PSD(f, x) f df}{\int PSD(f, x) df}, \quad (6)$$

where $PSD(f, x)$ represents the power spectral density of a small aperture beam propagated perpendicularly through the flow over a range of downstream distances defined by x . Eq. (6) yields a weighted average of the frequencies contained in the optical signal at each downstream location. This optical “natural” frequency may be used to determine the streamwise size of a statistically-probable aberrating vortical structure convecting downstream. This average structure size is called “optical coherence length” and is defined as

$$\Lambda_n = \frac{U_c}{f_n}, \quad (7)$$

where U_c is the convective velocity. Figure 2 shows the linear growth rate of the “optical coherence length” with respect to downstream distance for an unforced shear layer.

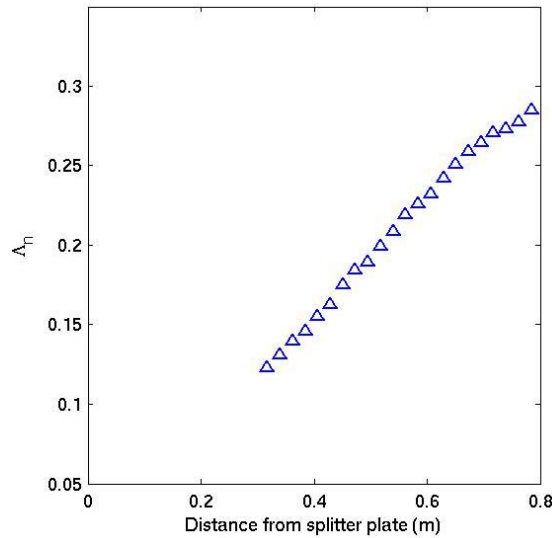


Figure 2. Optical coherence length versus downstream distance.

By applying forcing to the splitter plate, regularization of the otherwise irregular and unpredictable vortical structures may be obtained. A region of regularization is produced upstream from the location where the forcing frequency equals the optical “natural” frequency in the unforced case. Figures 3a, 3b, 3c, and 3d show single realizations of a model schlieren image overlaid by the shear-layer loci for each of the four different regularized shear layers that have been studied.

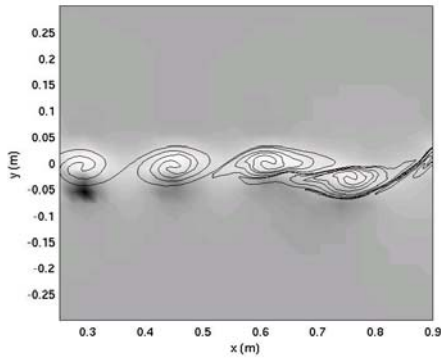


Figure 3a. $Ma_1 \sim 0.7$, $Ma_2 \sim 0.2$ simulated shear layer forced at a frequency of 900 Hz and amplitude of 5 mm.

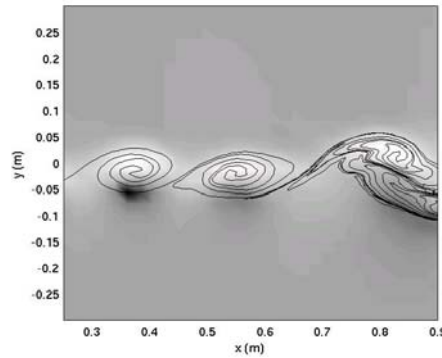


Figure 3b. $Ma_1 \sim 0.65$, $Ma_2 \sim 0.2$ simulated shear layer forced at a frequency of 650 Hz and amplitude of 5 mm.

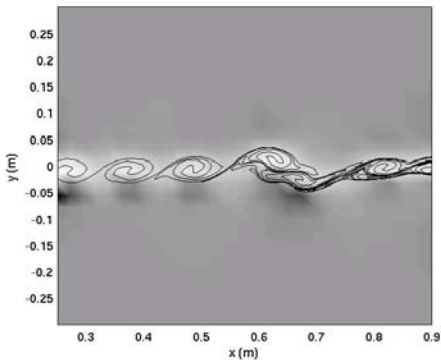


Figure 3c. $Ma_1 \sim 0.55$, $Ma_2 \sim 0.17$ simulated shear layer forced at a frequency of 1100 Hz and amplitude of 1 mm.

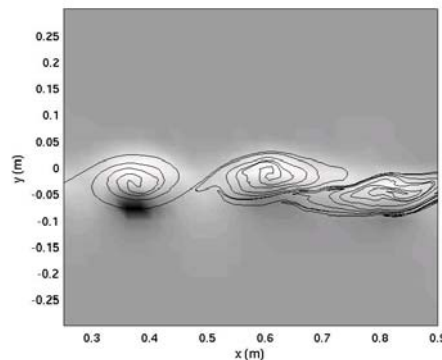


Figure 3d. $Ma_1 \sim 0.8$, $Ma_2 \sim 0.1$ simulated shear layer forced at a frequency of 650 Hz and amplitude of 5 mm.

IV. Alternative AO Control Approach

Traditional AO systems, comprised of a WFS, CC, and DM, sense and apply the appropriate corrections with the goal of minimizing the resulting wavefront aberrations. The bandwidth limitations associated with this feedback control system make traditional approaches to adaptive optics unrealistic in high speed applications.^{3,5} An alternative AO control approach discussed in this paper relies on two key components: regularizing the shear layer through flow control discussed previously, and applying AO corrections using a phase locked loop¹⁴ to perform feedback control. By regularizing the vortical structures, a more periodic and therefore predictable optical wavefront is produced. This wavefront can be approximated by a sinusoidal function and fed forward into the control system reducing the bandwidth requirement placed on the optical system. The amplitude is estimated using a feedforward technique while the phase of the DM wavefront is simultaneously being corrected via a phase locked loop.

In 2005, a flow-control-based AO experiment was conducted using a man-in-the-loop. Corrections were applied to a periodic aberration of 240 Hz with amplitude of $\sim 0.1 \mu\text{m}$. That experiment proved successful in correcting the optical aberrations, increasing the time averaged Strehl ratio from 0.64 without AO correction to 0.93 with AO correction.¹⁵ Figures 4a and 4b show the Strehl ratio results from the experiment.

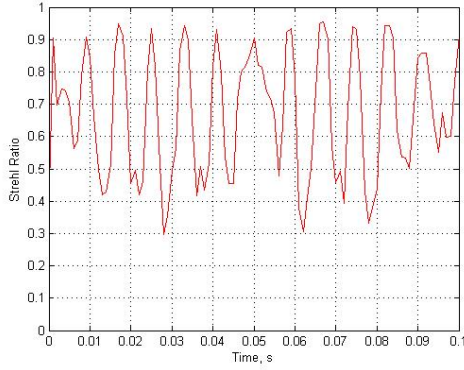


Figure 4a. Time history of Strehl ratio without correction.

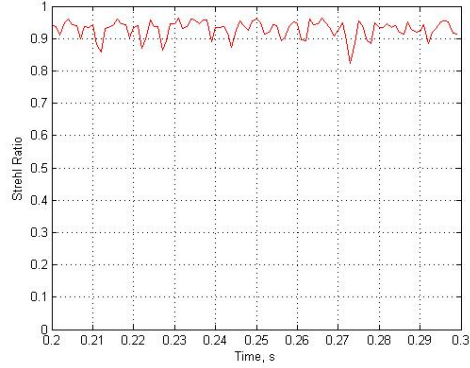


Figure 4b. Time history of Strehl ratio with correction.

A phase locked loop has been designed and simulated numerically based on this successful 240 Hz experiment using a man-in-the-loop. An actual analog control system, modeled after these simulations, is planned.

A. Simulated Experimental Setup

The simulated AO system consists of a DM comprised of thirty-seven piezoelectric actuators modeled two-dimensionally by seven rows of concurrent actuators, two small aperture position sensing devices, a feedforward control circuit and a feedback control circuit as shown in Figure 5.

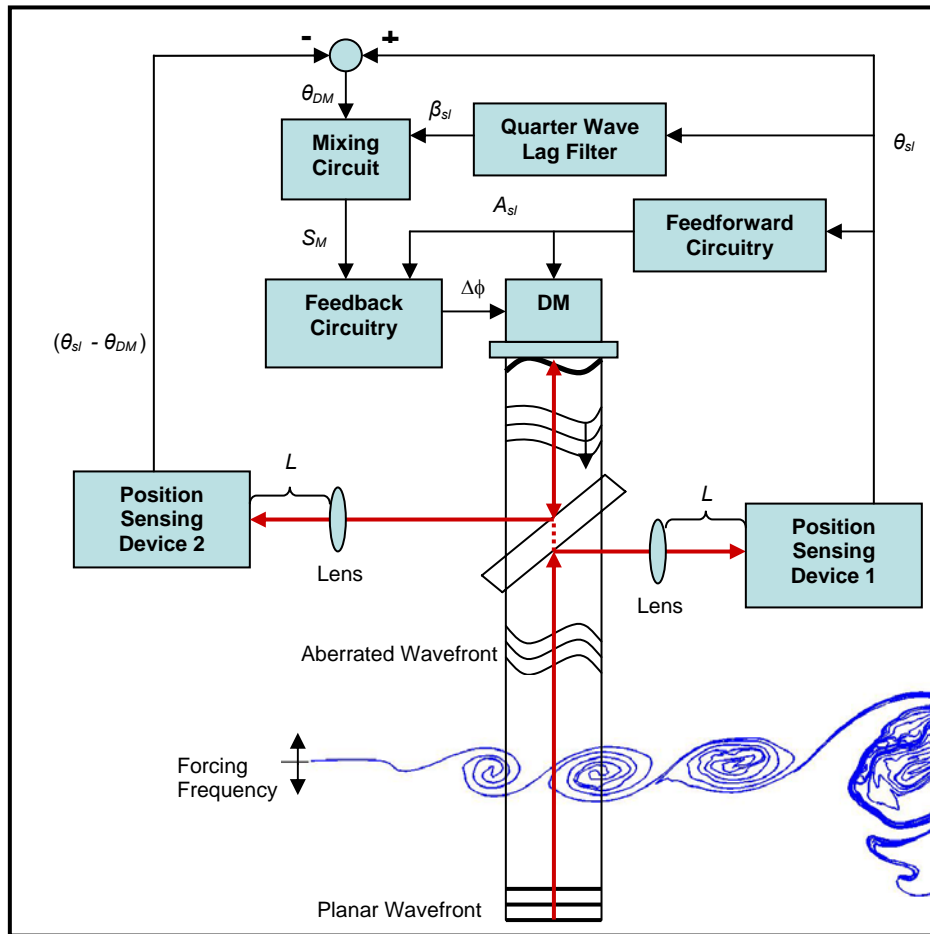


Figure 5. AO control system setup.

A small aperture laser beam associated with a planar wavefront is propagated through a shear layer that is being forced at a frequency, f_f , to regularize the vortical structures as described in the Section III. The emerging jitter signal (time varying signal due to aberrating wavefront) then passes through a beam splitter, directing part of the incident beam onto a position sensing device. The signal generated by this sensor is input into an analog feedforward circuit that estimates the amplitude of the aberrated wavefront. The signal is also used in the feedback circuitry to determine the phase difference between wavefronts. The part of the beam which passes through the beam splitter is reflected off the DM and redirected by the beam splitter onto another position sensing device producing a signal equivalent to the shear layer jitter minus the DM jitter ($\theta_{sl} - \theta_{DM}$). This signal is subtracted from the shear layer jitter signal to recover the jitter associated with the DM alone. The resulting signal (θ_{DM}) is mixed (multiplied) with the signal β_{sl} , a phase-shifted signal generated by passing the shear layer jitter signal, θ_{sl} , through a filter that has unit gain and a $\pi/2$ phase lag at the shear layer frequency, ω_{sl} . The resulting mixed signal is used to estimate the phase difference between the regularized aberrated wavefront and the DM wavefront. The estimated amplitude generated by the feedforward control circuit and the phase difference estimated by the feedback control circuit are used to drive the DM with the goal of minimizing the error between the regularized wavefront and the DM.

B. Phase Locked Loop

The objective of the control system is to drive the DM in such a way as to reduce the outgoing wavefront aberrations, increasing on-target intensity. Assuming the shear layer has been regularized and contains a single dominant optical frequency, the emerging wavefront will be akin to a traveling sinusoidal wave with an angular frequency,

$$\omega_{sl} = 2\pi f_f, \quad (8)$$

and wave number,

$$k_{sl} = \frac{\omega_{sl}}{U_c}, \quad (9)$$

where the convective velocity, U_c , is determined by cross-correlating two small aperture beams propagating perpendicularly through the flow¹⁶ a distance Δx apart with a time delay, τ :

$$U_c = \frac{\Delta x}{\tau}. \quad (10)$$

The shear layer's associated *OPD* will have an assumed form,

$$OPD_{sl}(t, x) = A_{sl} \sin(k_{sl}x - \omega_{sl}t + \phi_{sl}). \quad (11)$$

It is important to note that the only unknown parameters in Eq. (11) are the amplitude, A_{sl} , and phase, ϕ_{sl} , of the shear layer's optical wavefront. The known parameters, ω_{sl} and k_{sl} , will be used to drive the DM actuators whose corresponding *OPD* is defined as,

$$OPD_{DM}(t, x) = A_{DM} \sin(k_{sl}x - \omega_{sl}t + \phi_{DM}), \quad (12)$$

assuming the DM membrane can form the desired sine wave. In Eqs. (11) and (12), the subscripts '*sl*' and '*DM*' refer to *shear layer* and *deformable mirror* respectively. The goal is to use estimates of A_{sl} and ϕ_{sl} to determine the amplitude, A_{DM} , and phase, ϕ_{DM} , of the DM such that $|OPD_{DM} - OPD_{sl}|$ is minimized. This is accomplished using a feedback control system known as a phase locked loop¹⁴ (PLL). The PLL uses an estimate of the phase difference between the incident wavefront and the DM to synchronize the phase of

the DM's wavefront with the phase of the incident wavefront. Figure 6 shows a block diagram of the control system.

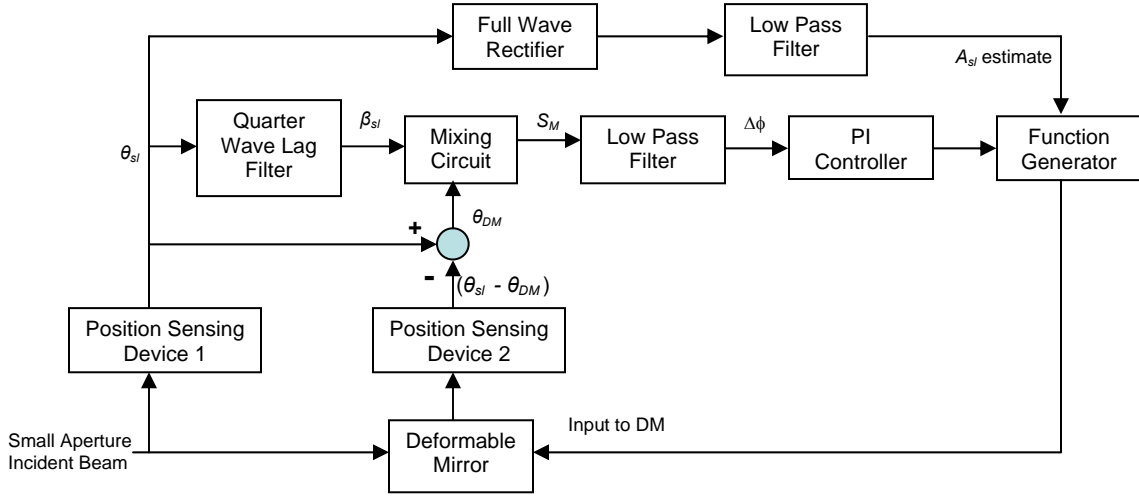


Figure 6. Block diagram of the control system.

According to Eq. (5), the jitter angles associated with the shear layer and the DM may be expressed as,

$$\theta_{sl}(t, x_o) = -A_{sl} k_{sl} \cos(k_{sl} x_o - \omega_{sl} t + \phi_{sl}) \quad (13)$$

and

$$\theta_{DM}(t, x_o) = -A_{DM} k_{sl} \cos(k_{sl} x_o - \omega_{sl} t + \phi_{DM}) \quad (14)$$

where θ_{sl} is measured via position sensing device 1 (located at the focal distance, L , of the lens shown in Figure 5), and θ_{DM} is the jitter angle corresponding to the location on the DM where the beam is reflected ($x = x_o$). The second position sensing device measures the jitter angle of a small aperture beam that propagates through the shear layer and reflects off of the DM producing a signal equivalent to the difference between θ_{sl} and θ_{DM} . This signal is subtracted from the shear layer jitter signal to recover θ_{DM} . The shear layer jitter signal, θ_{sl} , is passed through a quarter wave lag filter. This filter has a unit gain and applies a $\pi/2$ phase lag at the frequency, ω_{sl} . The shifted signal, β_{sl} , is then multiplied with θ_{DM} in a mixing circuit to generate the output,

$$\begin{aligned} S_M &= A_{DM} k_{sl} \cos(k_{sl} x_o - \omega_{sl} t + \phi_{DM}) A_{sl} k_{sl} \cos(k_{sl} x_o - \omega_{sl} t + \phi_{sl} - \frac{\pi}{2}) \\ &= \frac{A_{DM} A_{sl} k_{sl}^2}{2} \sin(2k_{sl} x_o - 2\omega_{sl} t + \phi_{sl} + \phi_{DM}) + \frac{A_{DM} A_{sl} k_{sl}^2}{2} \sin(\phi_{sl} - \phi_{DM}). \end{aligned} \quad (15)$$

The mixed signal, S_M , is composed of a D.C. bias whose magnitude is proportional to the sine of the phase difference between the DM and the incident aberrated wavefront. The mixed signal also contains a harmonic term at the frequency $2\omega_{sl}$. The PLL removes the second order harmonic using a low pass filter that will be implemented in analog circuitry using an RC circuit. The resulting signal consists of baseband signal components which have significantly lower bandwidths than the original jitter signals and whose amplitude is

$$A_{DC} \cong \frac{A_{DM} A_{sl} k_{sl}^2}{2} \sin(\phi_{sl} - \phi_{DM}). \quad (16)$$

The phase difference between the aberrated wavefront and the DM is extracted by rearranging Eq. (16) to produce

$$\Delta\phi = (\phi_{sl} - \phi_{DM}) = \sin^{-1}\left(\frac{2A_{DC}}{A_{DM}A_{sl}k_{sl}^2}\right). \quad (17)$$

This signal is then passed through a proportional integral compensator (which could also be easily implemented in analog circuitry) and used to control the DM so that the phase difference asymptotically goes to zero. The integral action in this compensator assures that the closed-loop system can asymptotically track step changes in the phase of the aberrated wavefront with zero tracking error. The use of proportional feedback adds a non-minimum phase zero in the control system's loop function which is required to assure the feedback system's closed loop stability.

Extracting the phase difference using Eq. (17) requires knowledge of the aberrated wavefront's amplitude, A_{sl} . This is accomplished using a position sensing device that measures the jitter angle of the aberrated wavefront before it hits the DM. The resulting jitter angle is then rectified and passed through a low pass filter to extract the amplitude of the jitter angle's DC component. The resulting signal is proportional to the amplitude of the aberrated wavefront and is used in Eq. (17) to determine $\Delta\phi$. The resulting phase error is then used to drive the DM in the required manner.

V. Simulation Results

The alternative AO control approach, described above, was applied to the four cases shown in Figures 3a, 3b, 3c, and 3d. Due to a combination of lower stream velocities and higher forcing frequencies, cases 1, 2, and 3 produced the most effective AO correction results. In cases 1 and 2, the selected forcing frequencies produced regions of regularization with highly periodic wavefronts. The single harmonic frequency present in each of these regularized wavefronts resulted in a successful PLL, significantly increasing the time-averaged on-target intensity. Figures 7a and 8a show the numerical time history of the on-target Strehl ratio for cases 1 and 2, before AO corrections are applied. Figures 7b and 8b show the numerical time history of the on-target Strehl ratios with AO corrections. In case 1, the time-averaged Strehl ratio (ratio of actual on-target intensity to diffraction limited on-target intensity) increased from 0.06 without AO correction to 0.85 with AO correction. In case 2, the time-averaged Strehl ratio increased from 0.16 without AO correction to 0.7 with AO correction. However, as shown in Figure 8b a few significant drops in the time-varying Strehl ratio still remained. These drops correspond to the beams diffraction pattern shifting off axis while maintaining a high intensity. In both simulations, a considerable increase in the on-target intensity occurred once the DM wavefront synchronized with the shear layer's aberrating wavefront. In each of these cases the response time is approximately 0.01 seconds, demonstrating the responsiveness this system would have to further changes in the aberrating wavefronts.

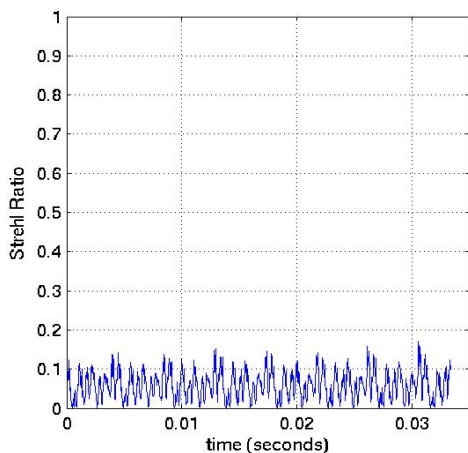


Figure 7a. Numerical time history of Strehl ratio for $Ma_1 \sim 0.7$ high speed side and $Ma_2 \sim 0.2$ low speed side without AO corrections.

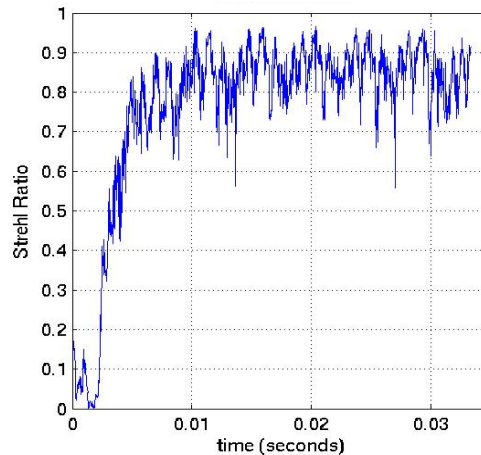


Figure 7b. Numerical time history of Strehl ratio for $Ma_1 \sim 0.7$ high speed side and $Ma_2 \sim 0.2$ low speed side with AO corrections.

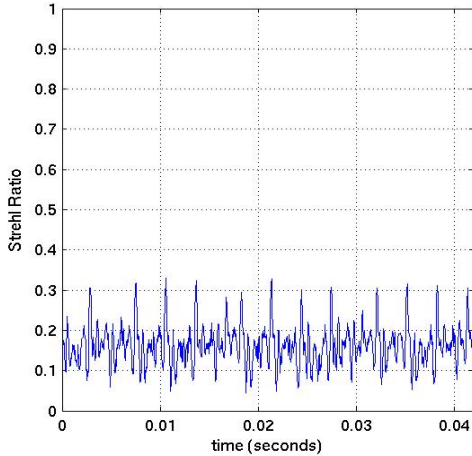


Figure 8a. Numerical time history of Strehl ratio for $Ma_1 \sim 0.65$ high speed side and $Ma_2 \sim 0.2$ low speed side without AO corrections.

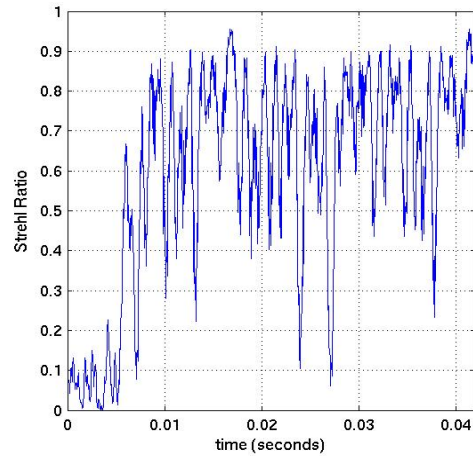


Figure 8b. Numerical time history of Strehl ratio for $Ma_1 \sim 0.65$ high speed side and $Ma_2 \sim 0.2$ low speed side with AO corrections.

Figures 9a and 9b show the numerical time history of the on-target Strehl ratio for case 3, without and with AO corrections. The combination of a lower convective velocity along with a high forcing frequency produced a regularized wavefront whose peak to valley amplitude was significantly less than the unforced case. This resulted in a substantial increase in the time-averaged Strehl ratio even before AO corrections were applied. Flow control alone produced a time-averaged Strehl ratio of 0.78 (Figure 9a). After AO corrections were applied the time-averaged Strehl ratio was raised to 0.95.

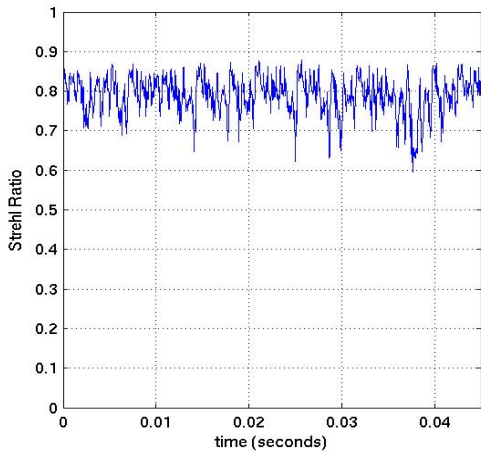


Figure 9a. Numerical time history of Strehl ratio for $Ma_1 \sim 0.55$ high speed side and $Ma_2 \sim 0.17$ low speed side without AO corrections.

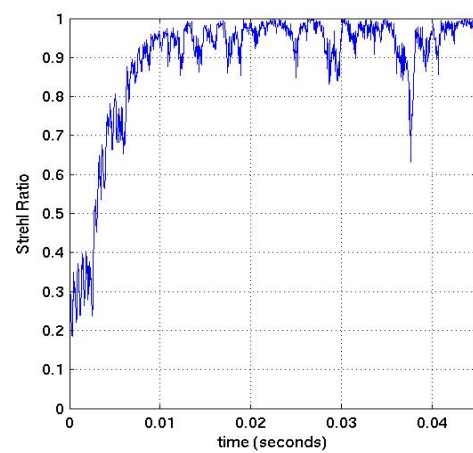


Figure 9b. Numerical time history of Strehl ratio for $Ma_1 \sim 0.55$ high speed side and $Ma_2 \sim 0.17$ low speed side with AO corrections.

Upon analyzing the time dependant intensity patterns for each of these three cases, it was noted that a large portion of the significant drops in Strehl ratio corresponded primarily to a shift in the diffraction pattern or intensity curve. This occurs when the OPD contains mostly tip/tilt error; the OPD has an average linear slope across the aperture. After adding a tip/tilt removal succeeding the AO corrections, the Strehl ratios for cases 1, 2, and 3 were increased even further as shown in Figures 10a, 10b, and 10c. In traditional AO systems, tip/tilt is removed prior to performing AO corrections; however this would result in a regularized optical wavefront resembling a standing wave rather than the desired traveling wave. Therefore, it became much more advantageous to perform tip/tilt removal after the AO corrections were implemented. Actual tip/tilt mirrors have a limiting bandwidth which must be considered when designing the final control system.

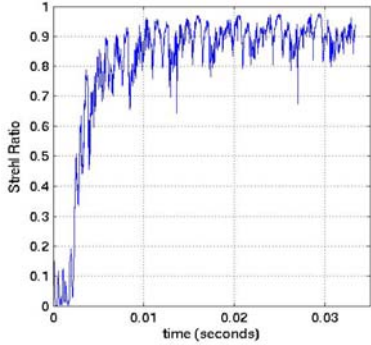


Figure 10a. Numerical time history of Strehl ratio for $Ma_1 \sim 0.7$ high speed side and $Ma_2 \sim 0.2$ low speed side with AO corrections and tip/tilt removed.

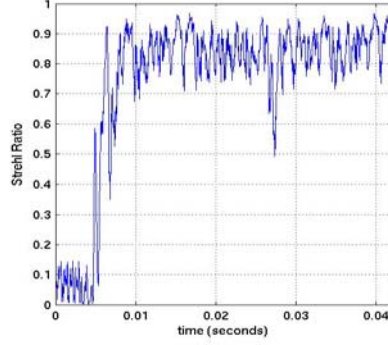


Figure 10b. Numerical time history of Strehl ratio for $Ma_1 \sim 0.65$ high speed side and $Ma_2 \sim 0.2$ low speed side with AO corrections and tip/tilt removed.

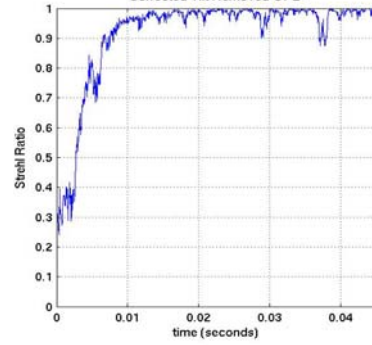


Figure 10c. Numerical time history of Strehl ratio for $Ma_1 \sim 0.55$ high speed side and $Ma_2 \sim 0.17$ low speed side with AO corrections and tip/tilt removed.

The final case studied for this paper was a Mach 0.8 high speed side, Mach 0.1 low speed side shear layer. The most effective forcing frequency for this case (case 4) was 650 Hz producing optical wavefronts containing both fundamental and subharmonic frequencies. This created inherent errors when trying to correct such aberrations using only a single frequency. In addition, the high convective velocity and low forcing frequency produces larger coherent vortical structures and larger peak to valley OPD amplitudes resulting in even lower initial Strehl ratios. Figures 11a and 11b show the time history of the Strehl ratios for this simulation. The time-averaged Strehl ratio increased from 0.07 without AO corrections to 0.26 with AO corrections. Research is currently being conducted to assess the possibility of using two-frequency mixing in order to recover a more appropriate DM waveform for this type of case. All four cases used a simulated beam aperture size of 0.18 meters and wavelength of 0.63 μm .

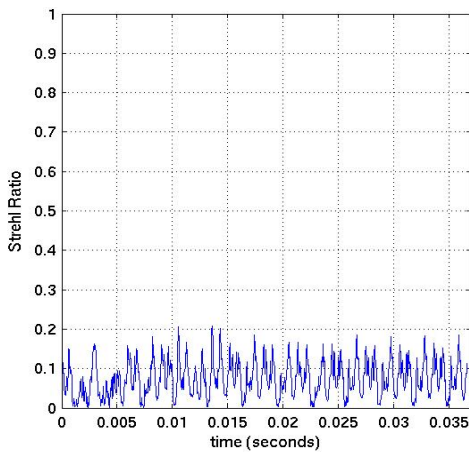


Figure 11a. Numerical time history of Strehl ratio for $Ma_1 \sim 0.8$ high speed side and $Ma_2 \sim 0.1$ low speed side without AO corrections.

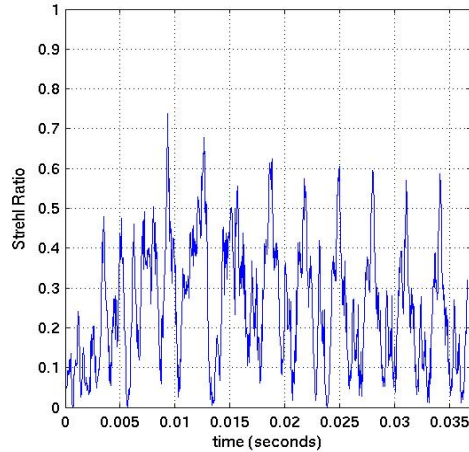


Figure 11b. Numerical time history of Strehl ratio for $Ma_1 \sim 0.8$ high speed side and $Ma_2 \sim 0.1$ low speed side with AO corrections.

VI. Conclusions

In an effort to overcome bandwidth limitations encountered by current AO systems, an alternative AO control system was designed and simulated based upon a successful man-in-the-loop experiment performed at Notre Dame.¹⁵ The simulations were performed numerically using a discrete vortex method coupled with a Weakly-Compressible model. Four different cases were studied with varying upper and lower Mach numbers. The shear layers were forced within their range of respective natural ‘optical’ frequencies achieving a region of regularized vortical structures and consequently more periodic optical wavefronts. Due to the single-frequency, periodic nature of the regularized wavefronts in three of the four cases, phase-locked-loop feedback control was successfully implemented to synchronize the DM wavefront with the

shear layer's aberrating wavefront. In the three cases dominated by a single frequency, the time-averaged Strehl ratios were increased from 0.06 to 0.85, from 0.16 to 0.7, and from 0.78 to 0.95. It was noted that a large portion of the remaining drops in on-target intensity was due to tip/tilt error. Upon removing this error, further increases in the simulated on-target intensity were achieved. Tip/tilt removal is typically performed prior to AO corrections however; this would result in a wavefront resembling a standing wave instead of the desired traveling wave. Therefore these additional corrections were applied after performing AO corrections. The last case studied in this paper revealed the need for two-frequency control in the event of a regularized wavefront containing both fundamental and subharmonic frequencies. Further research is being conducted to determine the appropriate means of controlling wavefronts containing more than one dominant frequency. The results obtained from this study will be further explored experimentally, and used to build an analog control system automating the AO corrections.

Acknowledgments

These efforts were sponsored by the Air Force Office of Scientific Research, Air Force Research Laboratory's Directed Energy and Air Vehicles Directorates, Air Force Material Command, USAF, under Grant Number F49620-03-1-0019. The U.S. Government is authorized to reproduce and distribute reprints for governmental purposes notwithstanding any copyright notation thereon. The authors are also grateful to the Directed Energy Professional Society for its support.

References

- ¹Kyrazis, D., "Optical degradation by turbulent free shear layers", *SPIE*, **2005**, 1993.
- ²Fitzgerald, E.J. and Jumper E.J., "The Optical Distortion Mechanism in a Nearly Incompressible Free Shear Layer," *Journal of Fluid Mechanics*, Vol. 512, 2004, pp. 153-189.
- ³Tyson, R.K., *Principles of Adaptive Optics*, 2nd ed., Academic Press, Chestnut Hill Massachusetts, 1991.
- ⁴Nightingale, A., Goodwine, B., Jumper, E. J., "Regularizing Shear Layer for Adaptive Optics Control Applications," *AIAA Paper 2005-4774*, Jun 2005.
- ⁵Cicchello, J.M., and E.J. Jumper, "Far-Field Optical Degradation due to Near-Field Transmission through a Turbulent Heated Jet," *Applied Optics*, **36** (25), pp. 6441-6452, September 1997.
- ⁶Duffin, D. A., "Feed-Forward Adaptive-Optic Correction of Aero-Optical Aberrations Caused by a Two-Dimensional Heated Jet," *AIAA Paper 2005-4776*, Jun 2005.
- ⁷Tsai, Y. P. and Christiansen, W. H., "Two-dimensional Simulation of Shear-Layer Optics", *AIAA Journal*, **28**, pp. 2092-2097, 1990.
- ⁸Inoue, O., "Vortex Simulation of a Turbulent Mixing Layer", *AIAA Journal*, **23**, pp. 367-373, 1985.
- ⁹Ashurst, W. T., "Numerical Simulation of Turbulent Mixing Layers Via Vortex Dynamics", *Turbulent Shear Flows I*, pp. 402-413, Springer, 1979.
- ¹⁰Fitzgerald, E.J., *The shear layer compressibility mechanism and its role in creating aero-optical distortions*, Dissertation, Notre Dame, 2000.
- ¹¹Jumper, E.J., and Hugo, R.J., "Quantification of Aero-Optical Phase Distortion Using the Small-Aperture Beam Technique," *AIAA Journal*, **33**(11), 1995, pp. 2151-2157.
- ¹²Chouinard, M. Asghar, A., Kirk, J.F., Siegenthaler, J.P. and Jumper, E.J., "An Experimental Verification of the Weakly-Compressible Model", *AIAA Paper 2002-0352*, Jan 2002.
- ¹³Oster, D. and Wagnanski, I., "The Forced Mixing Layer between Parallel Streams," *Journal of Fluid Mechanics*, **123**, 1982, pp. 91-130.
- ¹⁴Ziemer, R.E. and Peterson R.L., *Digital Communications and Spread Spectrum Systems*, MacMillan Publishing Co., New York New York, 1985.
- ¹⁵Duffin, D. A., Mansell, D., Jumper, E. J., "First Adaptive-Optic Correction of a 240 Hz Aero-Optic Aberration Using a Feed-Forward Approach," *8th DEPS Symposium*, Nov 2005.
- ¹⁶Gordeyev, S., Jumper, E.J., Ng, T., and Cain, A., "Aero-Optical Characteristics of Compressible, Subsonic Turbulent Boundary Layer," *AIAA Paper 2003-3606*, Jun 2003.